[59]A. D. B. Woods, W. Cochran, and B. N. Brockhouse, Phys. Rev. 119, 980 (1960).

[60]The minus sign is put in front of the expression for $e_{14}$ to make it agree with the accepted convention; see D. F. Nelson and E. H. Turner, J. Appl. Phys. 39, 3337 (1968). This convention puts the group-III atom at $(\frac{1}{4}, \frac{1}{4}, \frac{1}{4})$, which is opposite to our definition. The experimental values are negative for all III–V compounds measured so far (see Ref. 48), in contrast to the positive value used for GaAs in Refs. 25 and 55.

PHYSICAL REVIEW B VOLUME 3, NUMBER 4 15 FEBRUARY 1971

# Tunable Stimulated Raman Scattering from Mobile Carriers in Semiconductors

C. K. N. Patel and E. D. Shaw
*Bell Telephone Laboratories, Murray Hill, New Jersey* 07974

(Received 12 August 1970)

In this paper we discuss the recent results of stimulated Raman scattering (SRS) from mobile carriers in semiconductors. Single-particle as well as collective excitations of the electron gas in semiconductors can lead to tunable Raman scattering, which is of considerable interest. We show that some of the possible scattering mechanisms have Raman gain large enough to obtain tunable SRS. The specific case is our recent report of the first observation of tunable SRS in the infrared. This SRS process involves the spin flip of conduction electrons in InSb. Its frequency $\omega_s$ is tunable by varying a dc magnetic field $B$ as $\omega_s = \omega_0 - g\mu_B B$, where $\omega_0$ is the frequency of the pump, $g$ is the $g$ value of electrons, and $\mu_B$ is the Bohr magneton. With $Q$-switched $CO_2$ laser at 10.6 $\mu$ as the pump, the spin-flip Raman laser is tunable from 10.9 to 13.0 $\mu$ ($B \approx 15$–$100$ kG). The tunable coherent power is $\sim 10$ W for an input power of 1.0 kW. The tunable SRS has a linewidth of $\lesssim 0.03$ cm$^{-1}$ at $\omega_s \approx 800$ cm$^{-1}$ and its tuning linearity and resettability exceeds $1 : 3\times10^4$. We will discuss in detail the physics underlying the tunable SRS and describe the possible applications of such a tunable coherent radiation.

## I. INTRODUCTION

In this paper we discuss some of the experimental and theoretical results of stimulated Raman scattering (SRS) from conduction electrons in semiconductors. Studies of spontaneous Raman scattering from mobile carriers have shown that both the collective as well as the single-particle processes can give rise to tunable Raman shifts. In Secs. II and III, we evaluate the Raman gains for various scattering processes and show that for some of them, the calculated Raman gain (using the presently available lasers as pump) can be greater than optical losses in the semiconductor, and thus these processes should be eminently suitable for obtaining tunable stimulated Raman scattering.

In Sec. IV, we consider a specific case of the Raman scattering from the Landau level electrons in a semiconductor in a magnetic field, and we describe the experimental results of tunable SRS from spin flip of electrons in $n$-InSb.[1] The frequency $\omega_s$ of the spin-flip Raman laser varies as $\omega_s = \omega_0 - g\mu_B B$, where $\omega_0$ is the pump frequency, $g$ is the effective $g$ value of the conduction electrons, $\mu_B$ is the Bohr magneton, and $B$ is the dc magnetic field. Using a $Q$-switched $CO_2$ laser at 10.6 $\mu$ as the pump, the InSb spin-flip Raman laser can be tuned from $\sim 10.9$ to 13.0 $\mu$ by varying $B$ from $\sim 15$ to 100 kG. The linewidth of the tunable SRS is $\lesssim 4$ Å at $\sim 12.0$ $\mu$, corresponding to $\lesssim 0.03$ cm$^{-1}$ at $\sim 800$ cm$^{-1}$. The linearity and resettability of SRS frequency exceeds $1 : 3\times10^4$. Both the linewidth and linearity measurements, are, at present, limited by experimental techniques.

With a pump power of $\sim 1.0$-kW peak, tunable SRS power output is $\sim 10$ W. In Sec. V we discuss the limitations on the maximum spin-flip Raman laser power output and show that with $n$-InSb, the maximum power output is limited not by pump depletion but by saturation of the spin system taking into account the spin diffusion.

In Sec. VI, we discuss the tunability limitations of the spin-flip Raman laser and find that for a given electron concentration $n$-InSb, the lowest magnetic field for SRS is determined by the quantum limit for the upper-spin sublevel, while the upper limit on the magnetic field is determined by the free-carrier absorption. We also discuss the effect of varying the carrier concentration on the spin-flip SRS.

The very narrow linewidth and the extremely linear tunability of the spin-flip Raman laser points to many scientific and practical applications. In Sec. VII, we consider a particular case of infrared spectroscopy and show that the spin-flip Raman laser is superior to the conventional grating spectrometers in terms of resolution and speed.

Finally, in Sec. VIII, we summarize the paper by noting the implications of the very severe disturbance of the electron gas during SRS for studying nonequilibrium effects. We also indicate some avenues for future efforts and pose some problems not yet understood. We will also indicate some other Raman scattering processes where effects of a magnetoplasma lead to tunable Raman scattering and may be of interest.

## II. ELECTRONIC PROCESSES FOR TUNABLE RAMAN SCATTERING IN SEMICONDUCTORS

Study of spontaneous Raman scattering from mobile carriers in semiconductors is a fascinating subject on its own and has received great attention recently. Inelastic scattering of light from the various collective[2,3] as well as single-particle processes[4,5] has been theoretically predicted. Of the number of different Raman scattering processes experimentally and theoretically investigated, for our present discussions of stimulated Raman scattering we will restrict ourselves only to those which study collective effects involving optic plasmons and single-particle processes involving Landau level electrons in semiconductors. During Raman scattering from an elementary excitation such as those mentioned above, we are required to satisfy the energy and momentum conservation relations given in Eqs. (1) and (2):

$$\hbar\omega_s = \hbar\omega_0 \pm \hbar\omega_e \quad , \tag{1}$$

$$\vec{q}_s = \vec{q}_0 \pm \vec{q}_e \quad , \tag{2}$$

where $\omega_s$ and $\omega_0$ are the scattered and incident light frequencies, $\hbar\omega_e$ is the energy of the elementary excitation responsible for the scattering of light, $\vec{q}_s$ and $\vec{q}_0$ are the scattered and incident light wave vectors, and $\vec{q}_e$ is the wave vector of the above elementary excitation. The minus sign applies to Stokes-Raman scattering and the plus sign indicates anti-Stokes-Raman scattering.

For Raman scattering from optic plasmons,

$$\omega_e = \omega_p = (4\pi n e^2/m^*\epsilon_\infty)^{1/2} \quad , \tag{3}$$

where $\omega_p$ is the plasma frequency, $n$ is the carrier concentration, $e$ is the electron charge, $m^*$ is the effective mass, and $\epsilon_\infty$ is the high-frequency dielectric constant of the semiconductor. The cross section for Raman scattering from such an optic plasmon is given by[6,7]

$$\sigma_{\text{plasmon}} \approx (e^2/m^*c^2)^2 (q/q_{FT})^2 (\hbar\omega_p/E_F) \ \text{cm}^2\,\text{sr}^{-1} \quad , \tag{4}$$

where $q_{FT}$ is the Fermi-Thomas screening wave vector, and $E_F$ is the Fermi energy. For typical electron concentrations of $\sim 10^{16}$–$10^{17}$ cm$^{-3}$ in InAs, the cross section is $\sim 10^{-24}$ cm$^2$ sr$^{-1}$ per electron, and the plasma frequency is seen to vary from ~ 70 to 140 cm$^{-1}$. Thus, the optic plasmons are strong processes for obtaining tunable Raman scattering. Spontaneous Raman scattering from optic plasmons and plasmon-phonon coupled modes has been reported in GaAs [6] and from plasmons in InAs.[7] However, it should be realized that the "tuning" of the plasma frequency requires a change in the carrier concentration which can be accomplished by using semiconductor samples having different doping concentrations or by injection of excess carriers into the semiconductor. A more convenient technique for "tuning" the characteristic frequency of the collective excitation of the electron gas is application of a magnetic field to couple the plasmon and the cyclotron modes to give hybrid resonances of a magnetoplasma. Tunable spontaneous Raman scattering from such a magnetoplasma has been reported in GaAs.[8]

A far more promising method of obtaining tunable Raman scattering is the use of the single-particle processes involving the magnetic energy levels of the electrons in a semiconductor. Following theoretical predictions of Wolff[4] and Yafet,[5] spontaneous Raman scattering from such excitations in $n$-InSb has been reported.[9] Three distinct processes are observed corresponding to (i) a change of Landau level quantum number $l$ by 2 – the $\Delta l = 2$ transition (predicted[4]); (ii) a change of Landau level quantum number by 1 – the $\Delta l = 1$ transition (not predicted); and (iii) a change in the spin sublevel without a change in the Landau level quantum number – the spin-flip transition (predicted[5]). The frequencies of the Raman scattered light in the above cases is given by

$$\Delta l = 2; \quad \omega_s = \omega_0 \pm 2\omega_c \quad , \tag{5}$$

$$\Delta l = 1; \quad \omega_s = \omega_0 \pm \omega_c \quad , \tag{6}$$

$$\text{spin-flip}; \quad \omega_s = \omega_0 \pm g\mu_B B \quad , \tag{7}$$

where $\omega_c = eB/m^*c$ is the cyclotron frequency for the carriers. Figure 1 shows spontaneous Raman scattering results for electrons in InSb, where the tunability for the processes described in Eqs. (5)–(7) is large because of the small effective mass and the large $g$ value for the electrons. The order of magnitude of Raman scattering cross sections predicted for the $\Delta l = 2$ and the spin-flip processes are[4,5]

$$\sigma_{\Delta l=2} \approx (e^2/m^*c^2)^2 (\hbar\omega_c/\epsilon_g)^2 \ \text{cm}^2\,\text{sr}^{-1} \tag{8}$$

and

$$\sigma_{\text{spin-flip}} \approx (e^2/m_s^*c^2)^2 (\hbar\omega_0/\epsilon_g)^2 \ \text{cm}^2\,\text{sr}^{-1} \quad , \tag{9}$$

where $\epsilon_g$ is the band gap, and $m_s^*$ is the effective spin mass defined as $m_s^*/m_0 = 2|g|$, with $m_0$ equal to the free electron mass. The theoretical interpretation of the $\Delta l = 1$ transition is in doubt, and hence the scattering cross section is not given here (see Refs. 9–11). For the electrons in $n$-InSb,

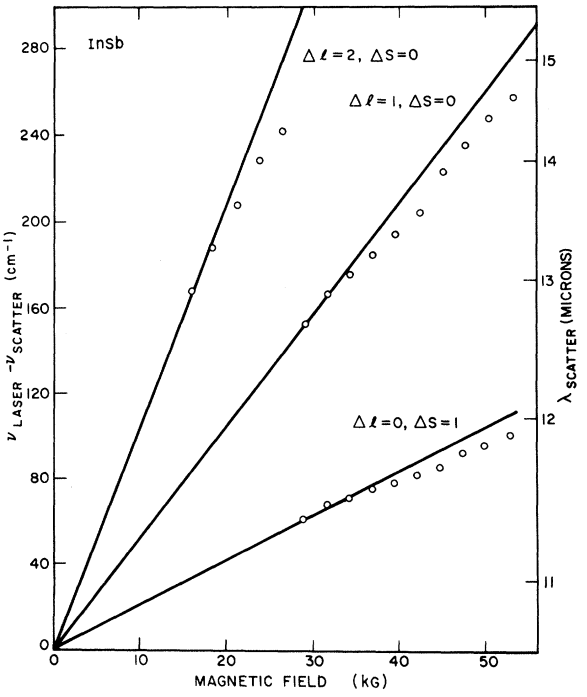


FIG. 1. Frequency shifts and positions of the spin flip, $\Delta l=1$ and $\Delta l=2$ spontaneous Stokes scattered light as a function of $B$ for $n$-InSb (Ref. 9).

the measured cross sections agree well with the calculated ones. These are

$$\sigma_{\Delta l=2}\approx\sigma_{\Delta l=1}\approx 10^{-24}\ \mathrm{cm^2\,sr^{-1}}$$

and

$$\Delta\sigma_{\mathrm{spin\text{-}flip}}\approx 10^{-23}\ \mathrm{cm^2\,sr^{-1}}$$

(Refs. 9 and 10). Thus the three single-particle magneto-Raman processes appear to be quite suitable for obtaining tunable stimulated Raman scattering. In particular, the spin-flip process in InSb is the most promising for achieving the stimulated Raman scattering because its cross section is at least an order of magnitude larger than either the plasmon Raman cross sections or the $\Delta l=1, 2$ Raman cross sections for materials which have been investigated so far.

### III. CALCULATION OF RAMAN GAIN

In order to proceed from spontaneous Raman scattering to stimulated Raman scattering, one requires a Raman gain large enough to overcome the optical losses in a Raman cavity. Raman gain is defined as the rate of growth of the number of photons in a given optical mode at the Raman shifted frequency. Optical gain $g_s$ arising from the Stokes-Raman scattering process is given[12] by

$$g_s=\frac{16\pi^2c^2(S/l\,d\Omega)}{\hbar\omega_s^3 n_p n_s(\bar{n}+1)\Gamma}\,I\ \mathrm{cm^{-1}}\quad,\tag{10}$$

where $S/l\,d\Omega$ is the Raman scattering efficiency in $\mathrm{cm^{-1}\,sr^{-1}}$, $I$ is the pump intensity in $\mathrm{W\,cm^{-2}}$, $\omega_s=\omega_0-g\mu_B B$ is the frequency of Stokes-Raman radiation, $n_{p,s}$ are the refractive indices at the pump and Stokes wavelengths, $(\bar{n}+1)$ is the Boltzmann factor in which $\bar{n}=(e^{g\mu_B B/kT}-1)^{-1}$, $T$ is the effective temperature, and $\Gamma$ is the full width of the spontaneous Raman line at half-height. For the present discussion, the Raman scattering efficiency $S/l\,d\Omega$ can be written as

$$S/l\,d\Omega=\sigma n_e\times f(E_F,B)\quad,\tag{11}$$

where $\sigma$ is the cross section for spontaneous Raman scattering, $n_e$ is the electron concentration, and $f(E_F,B)$ is a factor which describes the electron statistics; $f(E_F,B)\leq 1$ for magneto-Raman scattering, and $f(E_F,B)=1$ for plasmon scattering. As can be seen, to obtain a large Raman gain, a large scattering cross section $\sigma$ is desirable together with a small linewidth $\Gamma$ for the spontaneous Raman scattering.

It will be instructive to evaluate the gain in Eq. (10) for the different tunable Raman scattering processes discussed in Sec. II for various materials. For this purpose, we need to have a pump frequency $\omega_0$ in mind. Since we wish to compare materials such as GaAs, InAs, InSb, and PbTe which have different band-gap energies $\epsilon_g$, we will choose a pump frequency $\omega_0$ such that $\hbar\omega_0<\epsilon_g$ for the smallest gap. The $CO_2$ laser radiation at 10.6 $\mu$ satisfies this requirement. We will assume that the temperature $T$ is zero, the consequences of which will be discussed a little later. Also, for the magneto-Raman processes, we will assume that $f(E_F,B)\approx 1$, which is indeed true at very high magnetic fields. The crucial requirement for this assumption will be discussed in Sec. VI. With the above assumptions, we have calculated $g_s$ for plasmon and magneto-Raman scattering for materials in which these processes have been observed. The results are given in Tables I and II for InSb, InAs, and GaAs, and PbTe, respectively. Wherever possible, we have used the measured scattering cross sections and linewidths for the calculations. The results for InSb, InAs, and GaAs are straightforward to understand. The electron gas is isotropic, and thus the relative orientation of the magnetic field with respect to the crystal axes is largely unimportant in InSb, InAs, or GaAs. In PbTe, the results for which are given in Table II, the electron effective-mass tensor is anisotropic because the electrons are located in cigar-shaped valleys along the eight equivalent $\langle 111\rangle$ directions. The $g$ values for an electron, and consequently the spin masses in Eq. (9), depend upon the direction of the mag-

TABLE I. Calculated Raman gain $g_s/I$ ($cm^{-1}/W\,cm^2$) for the magneto-Raman and the plasmon Raman scattering in InSb, InAs, GaAs, and PbTe (pumped at 10.6 $\mu$).

| Scattering process | Semiconductor InSb [a] | InAs [b] | GaAs [c] | PbTe |
|---|---|---|---|---|
| Spin flip | $1.7\times10^{-5}$ | $1.3\times10^{-6}$ | d | see Table II |
| $\Delta l=1$ | $3.4\times10^{-7}$ | $3.6\times10^{-8}$ | d | d |
| $\Delta l=2$ | $5.7\times10^{-7}$ | $5.5\times10^{-8}$ | d | d |
| Plasmon | $(6\times10^{-7})$[e] | $1.2\times10^{-7}$ | $2\times10^{-9}$ | d |

[a] $n_e=3\times10^{16}$ $cm^{-3}$ for spin flip and plasmon, $B=50$ kG for spin flip; $n_e=5\times10^{16}$ $cm^{-3}$ for $\Delta l=1$, 2; $B=30$ kG.
[b] $n_e=1\times10^{17}$ $cm^{-3}$, $B=50$ kG.
[c] $n_e=1\times10^{17}$ $cm^{-3}$.
[d] Spontaneous Raman scattering data not available.
[e] Scattering cross section and linewidth calculated – spontaneous Raman scattering data not available.

netic field with respect to the $\langle 111\rangle$ valley in which the electron is located.[13] Thus, the Raman gain will depend upon the direction of the magnetic field with respect to the crystal axes as seen in Table II. (The calculated Raman gains for the $\Delta l=1$ and $\Delta l=2$ processes for GaAs and PbTe, as well as the spin-flip Raman process in GaAs and the plasmon Raman process in PbTe are not given because of the lack of experimental data on spontaneous Raman scattering cross sections and linewidths.) As remarked earlier, the spin-flip process should show the largest Raman gain because of its large cross section. An additional factor which makes the spin-flip Raman gain large is the very narrow linewidth for the process. As can be seen from Fig. 1 of Ref. 9, the spontaneously scattered spin-flip Raman line is significantly narrower than either the $\Delta l=1$ or the $\Delta l=2$ lines. Detailed measurements in InSb,[10] InAs,[7] and PbTe [13] have shown that while the $\Delta l=1$ and $\Delta l=2$ transitions have $\Gamma\approx 10-30$ $cm^{-1}$, the spin-flip transitions have consistently $\Gamma\leq 2$ $cm^{-1}$. The measured linewidths for plasmon-Raman scattering in GaAs [6] and InAs [7] are $\sim 10-20$ $cm^{-1}$ and are also considerably wider than those for spin-flip Raman scattering. The spin-flip Raman lines are very narrow because the electron collisions do not contribute to their widths. These narrow widths are primarily due to nonparabolicity of the conduction band (see the discussion in Sec. VI). Thus the enormous size of the Raman gain for the spin-flip Raman scattering compared to the gain from other scattering processes is understandable.

The absolute magnitude of the expected Raman gain is very large. Using a $Q$-switched $CO_2$ laser at 10.6 $\mu$, peak power output of $\sim 10$ kW is possible. (High peak power in the range of 10 MW is available at 10.6 $\mu$ from the high-pressure pulsed $CO_2$ lasers.[14,15]) Focusing this radiation into an area $\sim 10^{-3}$ $cm^2$ gives us an intensity $I\geq 10^7$ $W\,cm^{-2}$, and at least for the spin-flip Raman scattering in InSb and PbTe and perhaps in InAs, a possibility definitely exists for Raman gain to exceed the optical losses to achieve stimulated Raman scattering. The calculated Raman gain for the plasmon Raman scattering is also large enough to warrant an attempt to achieve stimulated plasmon Raman scattering in InAs and InSb. These somewhat lower gain Raman processes may require the use of the pulsed atmospheric pressure $CO_2$ lasers.

Before we proceed to the next sections dealing with experimental results, let us compare the spin-flip Raman gain with gain for Raman scattering from other elementary excitations, such as phonons, etc. The spin-flip Raman gain of $\sim 1\times10^{-5}$ $cm^{-1}/W\,cm^{-2}$ is the largest Raman gain known to date in any portion of the spectrum, and should be compared with the gain for Raman scattering in $CS_2$ at $\sim 5000$ Å. Carbon disulfide has one of the largest known Raman scattering efficiencies $S/l\,d\Omega$ for any material and is [16] $\sim 10^{-6}$ $cm^{-1}\,sr^{-1}$, which is larger than that for the spin-flip Raman process in InSb. In addition, the linewidth $\Gamma$ for $CS_2$ Raman scattering [16] is $\sim 1.4$ $cm^{-1}$ which is comparable to the linewidth for spin-flip Raman scattering. The calculated Raman gain [16] for $CS_2$ is, however, $\sim 1.3\times10^{-8}$ $cm^{-1}/W\,cm^{-2}$. The smallness of gain (as compared to that for the spin-flip Raman process) is a result of the $\omega_s^3$ factor in the denominator in Eq. (10) and is in part consequence of the fact that the number of optical modes per unit volume per unit frequency is inversely proportional to $\omega^2$. Thus, the use of a long wavelength pump laser to give a small $\omega_s$ is of a distinct advantage if $S/l\,d\Omega$ and $\Gamma$ are comparable at different wavelengths. For Raman scattering from phonons or molecular vibrations such as those in $CS_2$, unfortunately $S/ld\Omega$ is proportional to $\omega_0^4$, and in the final analysis $g_s$ will vary as $\omega_0$. However, for Raman scattering from electrons considered here, dependence of $S/l\,d\Omega$ on $\omega_0$ is much slower, e.g., for plasmon Raman and for spin-flip Raman processes $\sigma\propto\omega_0^2$ as seen from Eqs. (4) and (9), while for the $\Delta l=2$ magneto-Raman scattering $\sigma$ is nearly independent of $\omega_0$. Thus, even for the plasmon and spin-flip processes,

TABLE II. Calculated Raman gain $g_s/I$ ($cm^{-1}/W\,cm^{-2}$), for spin-flip Raman scattering in PbTe [a] (pumped at 10.6 $\mu$).

| Orientation | $\vec{B}\parallel\langle 111\rangle$ | | $\vec{B}\parallel\langle 110\rangle$ | | $\vec{B}\parallel\langle 100\rangle$ |
|---|---|---|---|---|---|
| Valleys | 2 at $\theta=0°$ | 6 at $\theta=70°32'$ | 4 at $\theta=35°32'$ | 4 at $\theta=90°$ | 8 at $\theta=54°44'$ |
| Gain | $1\times10^{-5}$ [b] | $3\times10^{-6}$ [c] | $1\times10^{-5}$ [b] | $1\times10^{-6}$ [c] | $1.1\times10^{-5}$ [c] |

[a] $n_e\approx 3\times10^{16}$ $cm^{-3}$.
[b] $B\approx 50$ kG.
[c] $B\approx 100$ kG.

the Raman gain increases as $\omega_s^{-1}$ and for the $\Delta l = 2$ process the gain increases as $\omega_s^{-3}$. Therefore, the use of a long-wavelength $CO_2$ laser is justified for SRS from electronic processes in semiconductors. (We have neglected any improvement in the quantity $S/l\,d\Omega$ that may arise from resonant effects due to a choice of $\omega_0$ close to $\epsilon_g$. Such a resonance enhancement[4,5] can be large and useful in lowering the pump power required to obtain SRS. One such possibility is the use of the CO laser[17] at 5.0–6.0 $\mu$ in the study of SRS from InSb. However, one also has to be aware of the increased absorption losses due to two-photon absorption and electron-hole pair production if very high intensity pump radiation is needed for appreciable Raman gain in spite of the resonance enhancement of the Raman scattering cross section, especially for some of the weaker Raman scattering processes.)

## IV. STIMULATED SPIN-FLIP RAMAN SCATTERING IN InSb

From the discussion in Secs. II and III, it is clear that the spin-flip Raman process in InSb has a substantial Raman gain, e.g., for a $3\times10^{16}$ cm$^{-3}$ sample,[1] $g_s \approx 1.7\times10^{-5}$ cm$^{-1}$/W cm$^{-2}$ at $B \approx 50$ kG. Thus, in order to estimate the pump intensity, we need to know the optical losses in the Raman cavity which have to be overcome to obtain SRS. The losses include a magnetic-field-independent reflection loss for the cavity, and a free-carrier absorption which depends upon the magnetic field in two ways. The first one is the $\lambda^2$ dependence of the free-carrier absorption since the spin-flip laser wavelength moves towards longer wavelengths with increasing magnetic field. The second one is that for $\vec{E} \perp \vec{B}$ and propagation normal to $\vec{B}$ (the geometry for the spin-flip Raman laser), the cyclotron absorption at the frequency of $(\omega_p^2+\omega_c^2)^{1/2}$ moves closer to the spin-flip Raman frequency. Both of these contributions to the free-carrier absorption can be easily obtained from the complex dielectric constant given below[18]

$$\epsilon(\omega) = \epsilon_\infty \left(1 + \frac{\omega_p^2[\omega_p^2 - \omega^2(1-i\eta)]}{\omega^2\{[\omega_p^2 - \omega^2(1-i\eta)](1-i\eta) + \omega_c^2\}}\right), \tag{12}$$

where $\epsilon_\infty$ is the high-frequency dielectric constant,

$$\omega_p = (4\pi n e^2/m^* \epsilon_\infty)^{1/2}$$

is the plasma frequency, $\omega_c = eB/m^*c$ is the cyclotron frequency, and $\eta = 1/\omega\tau$ in which $\tau$ is the electron collisional relaxation time. However, it can be seen that for InSb with mobility, $\mu \geq 1\times10^5$ cm$^2$/V sec and a carrier concentration of $\lesssim 3\times10^{16}$ cm$^{-3}$, the free-carrier absorption is also relatively field independent at $B \leq 50$ kG.

Figure 2 shows the two sample geometries which have been used. The geometry employed most commonly is seen in Fig. 2(a). The magnetic field is along the $z$ direction ($\vec{B}_z$). The incident pump radiation is propagating along the $y$ direction ($\vec{q}_{0y}$), and is polarized either parallel to the magnetic field ($\vec{E}_0 \parallel \vec{B}$), or perpendicular to the magnetic field ($\vec{E}_0 \perp \vec{B}$). The spin-flip Raman scattered light is resonated in the direction normal to both the pump-radiation propagation and the magnetic field ($\vec{q}_{sx}$). Thus, $\vec{q}_e = \vec{q}_0 - \vec{q}_s$ is also perpendicular to the magnetic field. This geometry will be called "$\vec{q} \perp \vec{B}$ noncollinear geometry." As can be readily argued, this is not the ideal geometry for obtaining stimulated Raman scattering since the Raman gain occurs only over the diameter of the pump beam, while the free-carrier absorption occurs over the entire length $l_c$ of the Raman cavity. A more desirable geometry for stimulated Raman scattering is shown in Fig. 2(b). Here the direction of the magnetic field, and the direction of propagation of the pump radiation, are the same as those for the sample geometry shown in Fig. 2(a). Now, however, the spin-flip Raman scattered radiation is resonated in the direction of the pump radiation ($\vec{q}_{sy}$). Here, again, $\vec{q}_e = \vec{q}_0 - \vec{q}_s$ is perpendicular to the magnetic field. But now the interaction between the pump radiation and the spin-flip Raman scattered radiation takes place over the entire length of the crystal in the $y$ direction. This geometry will be called the "$\vec{q} \perp \vec{B}$ collinear geometry." This, clearly, is more desirable geometry compared to that in Fig. 2(a). However, for observing spin-flip Raman scattered radiation below as well as above the threshold for stimulated Raman scattering, the $\vec{q} \perp \vec{B}$ noncollinear geometry of Fig. 2(a) is far more convenient because of the ease with which we can discriminate against the pump radiation. Thus, most of the experiments reported in the present paper were carried out using the $\vec{q} \perp \vec{B}$ noncollinear geometry of Fig. 2(a). In addition, the results reported here have been confined to the case of $\vec{E}_0 \parallel \vec{B}$ which is more desirable from the considerations that have to do with the dependence of the gain on the magnetic

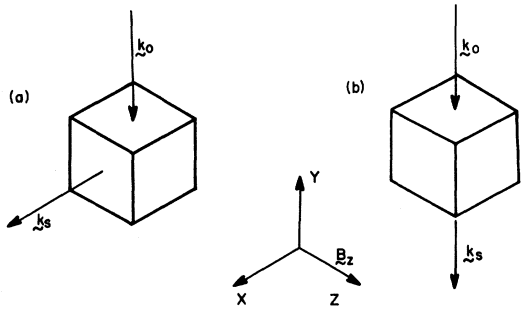


FIG. 2. Experimental geometry for observing stimulated spin-flip Raman scattering: (a) $\vec{q} \perp \vec{B}$ noncollinear; (b) $\vec{q} \perp \vec{B}$ collinear.

field. This is discussed in Sec. VI. The situations of $\vec{E}_0 \parallel \vec{B}$ in the $\vec{q} \perp \vec{B}$ noncollinear geometry as well as the $\vec{q} \perp \vec{B}$ collinear geometry of Fig. 2(b) have been successfully tried, and the results will be reported in a later publication.[19]

In Ref. 1, we estimated the total loss for an $n_e \approx 3 \times 10^{16}$ cm$^{-3}$ InSb sample in the $\vec{q} \perp \vec{B}$ noncollinear geometry with $\vec{E}_0 \parallel \vec{B}$ [Fig. 2(a)] to be ~1.5 Np (i.e., ~6 dB). This assumed that the Raman cavity was formed by normal specular reflections between the two parallel surfaces of the sample of length $l_c$. (A Raman cavity mode having substantially lower reflection losses would be a totally internally reflecting mode[20] which should be kept in mind when attempting a quantitative comparison between measured and calculated pump intensity required at threshold for stimulated Raman emission). In Ref. 1 we saw that even for the $\vec{q} \perp \vec{B}$ noncollinear geometry of Fig. 2(a), a modest focusing of a pump power of 1.5 kW into a spot 200 $\mu$ diam resulted in a Raman gain greater than the calculated losses, and experimentally tunable SRS from the electron spin flip in InSb was observed.

The experimental setup included a $CO_2$ laser which was repetitively $Q$ switched with a rotating mirror to give a pulse repetition rate of 120 Hz. The $CO_2$ laser had a diffraction grating inside the optical cavity to force the laser to oscillate on a single transition. Suitable apertures in the pump laser assured its operation in the lowest order transverse mode. The laser could be operated in two distinct modes: (a) a normal non-mode-locked operation when it produced peak power output of ~3–5 kW in pulses ~200–250 nsec wide; and (b) a mode-locked operation where the mode locking was produced spontaneously (i.e., without introducing a bleachable absorber inside the laser cavity), when it produced peak power output of ~6–10 kW in pulses ~5–10 nsec wide with a time separation of ~22 nsec between pulses, and with the 200–250-nsec envelope which is characteristic of the non-mode-locked output. The pulse shapes of these two pump pulses will be seen later. The wavelength of the output could be tuned for any of the strong $CO_2$ laser transitions with essentially the same power output. The pump laser radiation, so obtained, was focussed with a 30-cm focal length lens into a polished InSb sample in the appropriate geometry (see above). Typical sample length in the $\vec{q}_0$ direction was ~5 mm. The Raman scattered radiation was analyzed with proper long pass filters and 3/4-m grating spectrometer. A Ge : Cu detector was used. A variable pressure ether absorption cell in the pump beam path served as a variable attenuator to control the pump intensity.

In Fig. 3, we show the spin-flip Raman scattered output as a function of the 10.59-$\mu$ input power [obtained from a $Q$-switched $CO_2$ laser oscillating on the $P(20)$ transition] for a InSb sample with $n_e \approx 1.3 \times 10^{16}$ cm$^{-3}$ at $B = 40$ kG. The spin-flip laser radiation at 11.5 $\mu$ was isolated using long-wavelength pass filters. At low-input intensities we can see a spontaneous spin-flip Raman (SFR) scattering as evidenced by the linear variation of the spin-flip scattered output with the 10.6-$\mu$ input. At ~6 on the input scale, a sharp break occurs in the curve, and the SFR scattered power increases by ~$10^3$ with less than a twofold increase in the pump power, indicating that the Raman gain has become large enough to overcome the Raman cavity losses, and SRS from the spin flip of conduction electrons is obtained. In these experiments the maximum peak pump power inside the sample was ~1.0 kW, and the maximum peak output power was ~10 W. The threshold pump power for SRS is then seen to be at ~0.2 $P_{in}$(max), i.e., ~200 W. It should be noticed that this threshold is for a Raman

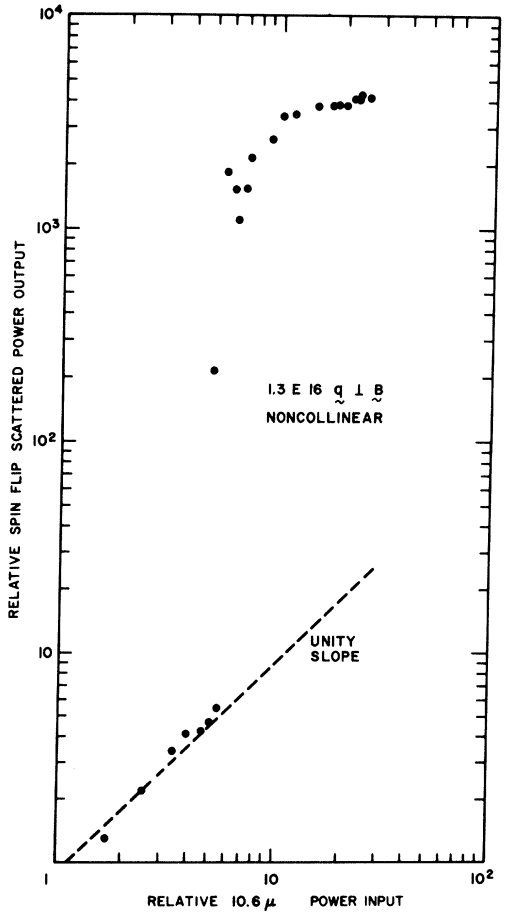


FIG. 3. SFR scattered power output at $\lambda \approx 11.5\,\mu$ as a function of pump power at 10.6 $\mu$ (in arbitrary units) for $n$-InSb with $n_e \approx 1.3 \times 10^{16}$ cm$^{-3}$, $T \approx 18$ °K and $B \approx 40$ kG. The maximum pump power is ~1.0 kW inside the sample and the maximum SFR laser output is ~10 W peak.

cavity whose reflectivity is determined by specular reflection of ~36% at the InSb surface. By using higher reflectivity dielectric coatings for the Raman cavity, one can remove almost all the reflection losses. The free-carrier absorption losses in the $1.3\times10^{16}$ InSb sample are very small, so the threshold pump power for SRS from such a coated sample should be lowered to tens of watts. This arrangement may allow cw operation of the tunable spin-flip Raman laser. The saturation of the SFR laser output for high input pump powers seen on Fig. 3. is believed to be real and will be discussed in Sec. V.

Another indication that stimulated Raman scattering is obtained can be seen in Fig. 4, where we show the spectral analysis of the SFR scattered output below and above SRS threshold. Below SRS threshold, we see a broad spontaneous line with a width of ~2 $cm^{-1}$. Above threshold, as expected, a significant narrowing of the line is seen (together with an enormously greater intensity). The width of the SRS line seen on Fig. 4 is spectrometer-resolution limited. Careful measurements with narrower spectrometer slits have failed to give any indication of the true width of the SFR laser output. However, by other techniques, we have been able to put an upper limit of ~0.03 $cm^{-1}$ on the SFR laser linewidth. It should be pointed out that linewidth can be calculated from spontaneous emission considerations using the expression[21]

$$\Delta\nu_{st} \approx 8\pi h\nu\,(\Delta\nu_{sp})^2/P \quad , \tag{13}$$

where $\Delta\nu_{st}$ is the linewidth of stimulated emission, $\nu$ is the frequency of laser oscillation, $\Delta\nu_{sp}$ is the is the spontaneous emission linewidth, and $P$ is the power output. With $\Delta\nu_{sp}\approx 2$ $cm^{-1}$ and $P\approx 10$ W, we obtain $\Delta\nu_{st}\approx 10$ Hz for cw operation. Thus the linewidth in the present case should be limited by the Fourier spectrum of the pulsed output and

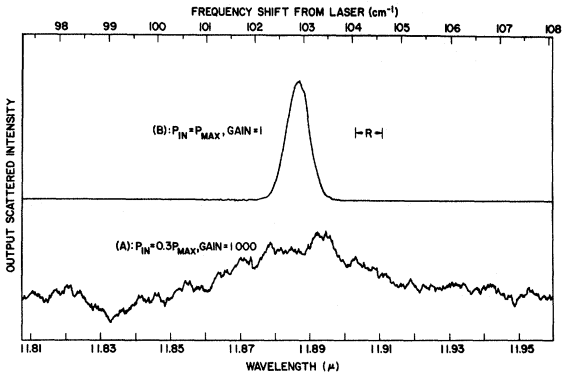


FIG. 4. Spectral analysis of SFR scattered power output below and above stimulated emission threshold (the gain in the figure refers to the amplifier gain) for $n$-InSb. $R$ is the spectrometer resolution.

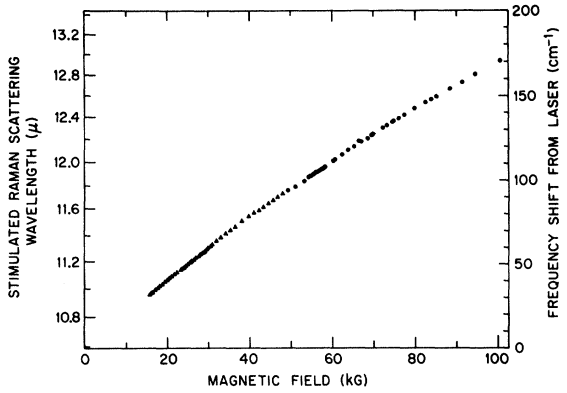


FIG. 5. Over-all tuning curve for the spin-flip Raman laser pumped with the $CO_2$ laser at 10.5915 $\mu$.

should be $\lesssim 10$ MHz. Under future cw operation of the SFR laser, the extremely narrow output of 10 Hz may be possible. Details of this discussion will be published elsewhere.[19]

The SFR laser frequency is tunable by varying the magnetic field as seen from Eq. (7). Figure 5 shows the over-all tunability of the SFR laser. The output wavelength can be tuned from 10.9 to 13.0 $\mu$ by varying the magnetic field from 15 to 100 kG, when using the $P(20)$ transition of the $00^01-10^00$ band of $CO_2$ at 10.5915 $\mu$ as the pump. The tuning limitations will be discussed in Sec. V. We have been able to extend the tuning range somewhat by using different transitions from the $CO_2$ laser as the pump,[22] e.g., by using the $CO_2$ laser pump at 10.23 $\mu$ [$R(22)$ transition] we have obtained SFR laser output at ~10.6 $\mu$, and by using the $CO_2$ laser pump at 10.8 $\mu$ [$P(40)$ transition] we have obtained a spin-flip laser output at 13.2 $\mu$.[19] In any case, the large $g$ value of electrons allows us to obtain a very respectable amount of over-all tuning of the SRS from the spin flip of electrons in InSb.

An important question concerns the fine tuning of the SFR laser wavelength. This feature determines the ultimate usefulness of any tunable source of coherent radiation. We have a Raman cavity of length $l_c\approx 2$ mm having a finesse[23] $\approx 2$–3, and cavity-mode separation of ~0.625 $cm^{-1}$. When the magnetic field is varied, the spontaneous SFR line (i.e., the Raman gain curve) having a width of $\approx 2$ $cm^{-1}$ sweeps through the cavity resonances. The spin-flip Raman laser will oscillate at those frequencies where Raman gain exceeds the cavity losses. Thus normally one would expect the SFR laser to oscillate at frequencies close to the cavity resonances giving rise to significant amount of frequency pulling/pushing.[21] Experimentally, we found that at any given time, SFR laser output occurred in only one line having width $\lesssim 0.03$ $cm^{-1}$, and no evidence of simultaneous oscillation on two Raman cavity

modes was found. A very careful measurement of the output wavelength as a function of $B$ as the SFR line is swept through tens of Raman cavity modes, showed no indication of the SFR laser frequency jumping from one cavity mode to the next. To our great surprise, the SFR laser frequency tracked linearly with the magnetic field to the best accuracy we can measure using a spectrometer. The only nonlinearity in tracking seen was the nonuniformity of spectrometer drive screw which amounted to $\sim 0.03$ cm$^{-1}$ with a periodicity of $\sim 1.5$ cm$^{-1}$, i.e., completely different from the expected periodicity of $0.625$ cm$^{-1}$ for the Raman cavity. Thus, we can say with confidence that the linearity and resettability of the SFR laser frequency is better than $0.03$ cm$^{-1}$. Of course, such a linearity of tuning and complete lack for frequency pulling/pushing by the cavity modes immensely increases the usefulness of a tunable laser source (as opposed to the tunable $Pb_{1-x}$ $Sn_x$ Te diode lasers which can only be tuned approximately a few GHz about each cavity mode before mode jumping occurs[24]), but it also makes the understanding of the phenomenon quite difficult. A part of the answer to the complete absence of frequency pulling/pushing by the Raman cavity modes may lie in the fact that the Raman cavity has a poor finesse as mentioned above. But this does not appear to be the complete answer and the matter is under further study.[19] The experimental evidence that in spite of the lack of frequency pulling/pushing by the Raman cavity, the SFR laser does indeed see the Raman cavity comes from the variation of the SFR laser output power as its frequency is tuned over a few cavity modes. We observe a 10–20% modulation in the output amplitude with a periodicity of $0.631$ cm$^{-1}$ which agrees very well with the expected Raman cavity mode separation. A theoretical argument in favor of the resonant SFR laser operation rather than nonresonant superradiant SFR emission comes from considering the narrowing of a spontaneous emission line that is expected during superradiance. This narrowing depends upon the profile of the spontaneous emission line, which is not known with any accuracy for the spin-flip Raman process (see the discussion on the line shape in Sec. VI). For the two simple line shapes, the Lorentzian and the Gaussian, the line narrowing due to superradiance is given by (i) Lorentzian line shape:

$$\Delta\nu_{sup} = \Delta\nu_{sp}/[(\alpha l/\ln 2) - 1]^{1/2} \quad ; \tag{14}$$

(ii) Gaussian line shape:

$$\Delta\nu_{sup} = \frac{\Delta\nu_{sp}}{(\ln 2)^{1/2}} \left[\ln\left(\frac{\alpha l}{\alpha l - \ln 2}\right)\right]^{1/2} \quad , \tag{15}$$

where $\Delta\nu_{sup}$ is the width after superradiance, $\Delta\nu_{sp}$ is the spontaneous emission linewidth, and $\alpha l$ is the total gain in the amplifying medium. Even though we do not know the exact line shape for the spontaneous SFR emission, we can attempt to compare the observed SFR laser linewidth with the superradiant linewidth for the two characteristic line shapes described above. For SFR scattering, $\Delta\nu_{sp} \approx 2$ cm$^{-1}$. For reaching a SFR power output of $\sim 10$ W starting from approximately one photon at the SFR frequency, we need $\alpha l \approx 50$. Thus, for a Lorentzian line the $\Delta\nu_{sup} \approx 0.24$ cm$^{-1}$, and for a Gaussian line the $\Delta\nu_{sup} \approx 0.28$ cm$^{-1}$. Both of these are significantly larger than the observed SFR laser linewidth of $\lesssim 0.03$ cm$^{-1}$, indicating that it is highly unlikely that we could be observing mere nonresonant superradiant SFR emission even though the SFR laser frequency shows no pulling/pushing by the Raman cavity modes. Further explanation of this phenomenon will be given elsewhere.[19]

## V. SPIN-FLIP RAMAN LASER POWER OUTPUT SATURATION

The maximum spin-flip Raman laser power output was obtained from the $n_e = 1.3 \times 10^{16}$ cm$^{-3}$ InSb sample having an electron mobility $\mu = 2.4 \times 10^5$ cm$^2$/V sec. In Fig. 3, we saw that a distinct saturation of the SFR laser power occurred at high input power levels. This saturation is believed to be real and cannot result from pump depletion since the SFR laser output is only $\sim 10$ W compared to the maximum input power of 1.5 kW. The saturation of the output power is confirmed by comparing the time dependence of the output pulse with that of pump pulse shown in Fig. 6 for both the normal operation of the $CO_2$ laser and for the mode-locked operation. The non-mode-locked laser pulse is seen to be $\sim 150$ nsec wide at half-height. Since the SFR laser threshold occurs at $\sim 0.2\ P_{in}$ (max), the spin-

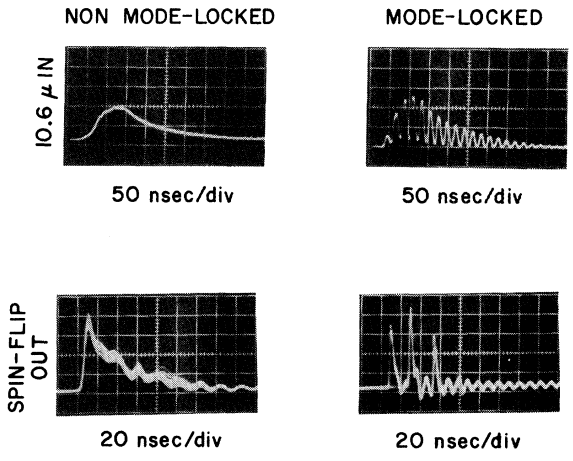


FIG. 6. Input $CO_2$ laser pulses and output spin-flip Raman laser pulses for normal operation and for mode-locked operation of the $CO_2$ laser ($n$-InSb, $n_e \approx 1.3 \times 10^{16}$ cm$^{-3}$, $T \approx 18$ °K, $B \approx 40$ kG).

flip Raman laser should oscillate for ~200–225 nsec. The SFR laser output in the picture below shows that it operates for ~80 nsec. It is also seen that the spin-flip laser output rises very rapidly and then decays with a time constant of ~30–35 nsec. This rapid decay is not surprising when considering the saturation of the electron spin system, i.e., the spins not being able to relax from the spin-down sublevel back to the spin-up sublevel rapidly enough. The spin saturation effectively decreases the Raman gain and eventually the SFR laser emission stops even before the laser pulse has decayed down to a level where we would have expected the turn off of the SFR laser from simple threshold considerations. The decay time of the spin-flip Raman laser output, however, does not simply give the spin-relaxation time because of the diffusion of the spins in and out of the focussed $CO_2$ laser beam, i.e., the spin-down electrons diffusing out from the $CO_2$ laser beam and the spin-up electrons diffusing into the beam to reduce the reduction in gain due to spin saturation. The spin-relaxation time is expected to be long compared to the pump pulse duration, and thus, the decay time of spin-flip laser pulse describes diffusion. As can be expected, the decay is nonexponential. We can calculate the number of spins which can contribute to the spin-flip Raman laser output with diffusion and compare that with the number of photons emitted in each spin-flip Raman laser pulse. With a peak power of ~10 W, for the pulse shown on Fig. 6, we have $\sim 2\times10^{13}$ photons. With a pump laser beam diameter of ~200 $\mu$ and a crystal length of ~4 mm, the solution of the diffusion problem with the transient pump pulse shows that the number of up spins that interact with the pump laser to give stimulated Raman scattering is $\sim 1\times10^{14}$. This is an acceptable agreement between theory and measurement considering the nature of the diffusion problem. The case of the spin-flip Raman laser with mode-locked excitation is very much more involved and will not be discussed quantitatively; but, here again, the spin saturation is quite evident.

In order to increase the SFR laser output, then, it is necessary either to reduce the spin-relaxation time or to increase diffusion of spins. There are ways of reducing the spin-relaxation time such as introduction of a paramagnetic impurity into InSb; however, it is doubtful if such a technique will not ruin the otherwise good optical quality of the crystal needed for low-loss operation. The idea of increasing the diffusion rate is somewhat more appealing. This can be easily accomplished by drifting the carriers normal to the direction of pump laser propagation. At reasonably attainable drift velocities of the order of $10^7$–$5\times10^7$ cm/sec, the effective spin-relaxation rate is $\sim 10^{-9}$–$10^{-10}$ sec (assuming a pumped region ~200 $\mu$ in diameter). This will increase the saturation power level by a factor of 10–100. Another technique of increasing the spin-relaxation rate is to work with a multivalley semiconductor such as PbTe to obtain SFR laser and use the intervalley electron transfer as a way of obtaining fast spin relaxation. This will be discussed in Sec. VIII.

## VI. LIMITATIONS ON TUNABILITY OF SFR LASER

In Ref. 1, we saw that for a $3\times10^{16}$ cm$^{-3}$ InSb sample SRS by the electron spin flip could not be obtained at $B$ less than ~48 kG corresponding to a wavelength of ~11.7 $\mu$. However, in Sec. IV, we saw from Fig. 5 that the lower magnetic field limit is now at ~15 kG with a corresponding tunability of the SFR laser wavelength from 10.9 $\mu$ to ~13.0 $\mu$. This extension of the low-field limit was accomplished by using lower carrier concentration samples. A definite $B_{min}$ is required in order to obtain SRS from a given carrier concentration sample even with the maximum input pump power. A typical SFR scattered power output vs $B$ curve is shown in Fig. 7 for $n_e \approx 1.3\times10^{16}$ cm$^{-3}$ sample. For $B \leq 26$ kG only spontaneous SFR scattering is observed which is seen to increase slowly as $B$ is increased in agreement with earlier[10] spontaneous SFR scattering results. At $B \approx 26$ kG, the SFR scattered output increases very suddenly by $\sim 10^4$ and SRS is observed. This $B_{min}$ required is seen to be smaller as carrier concentration is lowered. In this section we give a quantitative explanation for the existence of this low-field limit for SFR laser operation. We also discuss the high-field limit and the dependence of the SFR laser power output on the carrier concentration and the magnetic field.

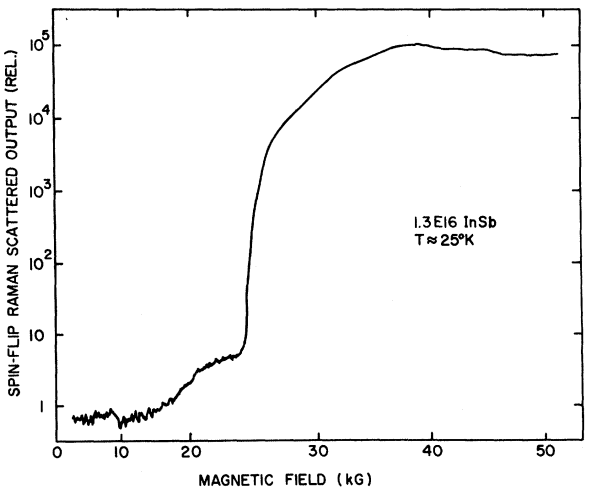


FIG. 7. SFR scattered power output as a function of magnetic field for $n$-InSb with $n_e \approx 1.3\pm10^{16}$ cm$^{-3}$, $T = 25$ °K, and at maximum pump power.

As mentioned earlier,[1] the threshold for SRS is determined by the gain available to overcome the optical losses in a Raman cavity. The optical gain is obtained from Eqs. (10) and (11), and the free-carrier absorption is obtained from Eq. (12). Since the Raman cavity reflection losses are independent of $n_e$ and $B$, all the SFR laser power output as well as SFR laser threshold dependence on $n_e$ and $B$ must arise from Eqs. (10)–(12).

Let us first discuss the magnetic field dependence (although the carrier concentration dependence is also tied in with the $B$ dependence) of the SRS threshold. The Raman gain in Eqs. (10) and (11) is proportional to $S/l\, d\Omega$ which depends on the magnetic field from two factors. The first is the slow dependence of $\sigma$ on $B$ (Ref. 5) and the second is the $f(E_F, B)$ which is field dependent in the case of degenerate electron statistics. In Fig. 8(a), we show the electron energies in InSb as a function of $k_z$ (electron momentum along the $z$-directed magnetic field) at $B \approx 20$ kG. We also show the Fermi energy $E_F$ for a carrier concentration of $\sim 3\times10^{16}$ cm$^{-3}$. It is seen that the upper-spin level (the spin-down level) of the $l=0$ Landau level is partially filled, and since during SFR scattering process an electron from the spin-up sublevel is excited to an empty state in the spin-down sublevel, only the electrons near the Fermi surface will be able to participate, making $f(E_F, B) < 1$. The situation is significantly more serious than what it appears because the density of states for the conduction electrons has a singularity[25] at $k_z = 0$. Thus, an exceedingly small fraction of the electrons in InSb are capable of giving rise to SFR scattering and $f(E_F, B) \ll 1$ [for the case shown in Fig. 8(a)] unless all the electrons happen to be in the lowest-spin sublevel as shown in Fig. 8(b) where we have increased the magnetic field to 50 kG while keeping the same $n_e$. Here $f(E_F, B) \approx 1$. This is precisely the quantum limit for the spin-down sublevel[25] in the conduction band. This implies that $S/l\, d\Omega$ will be increasing as $B$ is increased until we reach the quantum limit, as long as the $B$ dependence of $\sigma$ can be neglected. In the low magnetic field regime, this has been verified both experimentally[10] and theoretically.[26] (For high magnetic fields in the range of 100 kG, the above approximation of neglecting $B$ dependence of $\sigma$ is not valid and, as we shall see, it should have an effect on the behavior of high carrier concentration samples which require high magnetic fields to reach the quantum limit.) Thus, the electron statistics are expected to give a strong magnetic field dependence to the Raman gain. The magnetic field required to reach the quantum limit depends on the carrier concentration through its dependence on the Fermi energy which is also a function of magnetic field.[25] The quantum limit is reached at progressively lower magnetic fields as the carrier concentration is reduced.

Since we are discussing the low-field limit for Raman threshold, additional magnetic field dependence can also come from the Boltzmann factor $\bar{n}$ for the effect of lowering the field is to reduce $g\mu_B B$ towards zero. In practice, the Boltzmann factor can be neglected as long as $g\mu_B B \gtrsim 2kT$. In the experiments to be reported here, the sample

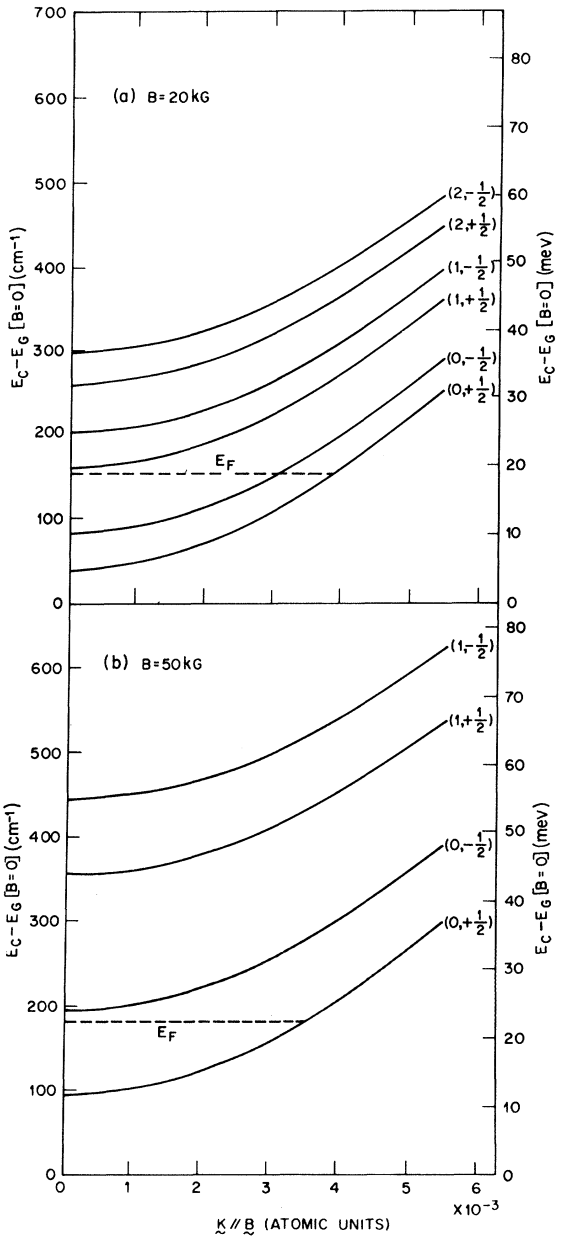


FIG. 8. (a) Landau level energies in $n$-InSb vs $k_z$ at $B = 20$ kG. We also show Fermi energy for $n_e \approx 3\times10^{16}$ cm$^{-3}$; (b) same as (a) but at $B = 50$ kG, showing the spin-down sublevel just emerging from the Fermi sea.

temperature was in the range of ~20 °K corresponding to $kT \approx 16$ cm$^{-1}$. Thus we can neglect the Boltzmann factor for $B \geq 15$ kG for InSb. For operation at lower magnetic fields, it is clear that the sample temperature should be lowered. An additional magnetic field dependence of the Raman gain arises from the $(\omega_s)^3$ term in the denominator of Eq. (10). However, for the range of magnetic fields considered here, this variation is very slow. Thus, the net effect of the above discussion is that as long as $g\mu_B B \geq 2\ kT$, the $B_{\min}$ for stimulated SFR scattering is governed by the quantum limit for the spin-down sublevel.

Another effect of the singularity in the density of states is seen in the spontaneous spin-flip Raman scattering linewidth which is determined primarily by the nonparabolicity of the conduction band. Here we have assumed that the $\vec{q}_e = \vec{q}_0 - \vec{q}_s$ is normal to the magnetic field, and consequently the contribution to the spontaneous SFR linewidth from a change in $k_z$ can be neglected. (See, for example, Fig. 23 of Ref. 10, where $\vec{q}_e$ is not wholly perpendicular to $\vec{B}$ and the contribution to the spontaneous SFR linewidth has to be taken into account.) Figure 9 shows the calculated nonparabolicity width for the $n_e \approx 1.3 \times 10^{16}$ cm$^{-3}$ InSb sample as a function of magnetic field and as defined on the inset. We have also assumed that the electron gas remains degenerate even at the highest magnetic field, where the Fermi energy becomes a small fraction of the Fermi energy at zero magnetic field. The width shown in Fig. 9 would be the total width of the spontaneous SFR line if the density of states were to be uniform as a function of $k_z$. The singularity in the density of states at $k_z = 0$ makes the spontaneous SFR line stronger for the largest frequency shift at a given magnetic field, i.e., the spontaneous SFR line strength is weighed towards contributions coming from electrons at small $k_z$. The ultimate result is to make the spontaneous SFR line narrower than that seen in Fig. 9. In addition, the spontaneous SFR emission line will be unsymmetrical, reflecting the density of states. Experimental measurements of spontaneous SFR linewidth of $\approx 2$ cm$^{-1}$ qualitatively confirm the former, at least at intermediate magnetic fields. For quantitative comparison of the measured and the calculated linewidths, however, level broadening effects have to be included in evaluating the narrowing of the spontaneous SFR linewidth due to the singularity in the density of states at $k_z = 0$. In any case, this will make the spontaneous SFR line narrower as the magnetic field is increased. From Eq. (10), it can be seen that the Raman gain should benefit from the decreasing linewidth at higher magnetic fields. In practice, however, we have seen little variation in the spontaneous SFR emission linewidth $\approx 2$ cm$^{-1}$ as the magnetic field is increased from ~40 to 100 kG. Notice that a linewidth of 2 cm$^{-1}$ at 100 kG is greater than that calculated in Fig. 9 which did not take into account the narrowing due to the density of states. This apparent discrepancy is understood to be arising from the fact that for magnetic fields larger than ~70 kG, the electron gas in the $n_e \approx 1.3 \times 10^{16}$ cm$^{-3}$ InSb sample is no longer degenerate at sample temperature in the range of 20–30 °K. Efforts are under way at present to include the effects of level broadening and finite temperature for evaluating the spontaneous SFR emission linewidth and the line shape as a function of magnetic field, and the results will be reported elsewhere.[19]

Let us now look at the high-field limitations on SFR laser (apart from those imposed by a finite magnetic field available in a given laboratory). The high-field limit is jointly set by the gain and the free-carrier absorption. Because of the dependence of $\sigma$ on $B$, for $\vec{E}_0 \| \vec{B}$ and $\vec{E}_0 \perp \vec{B}$ (see Fig. 1 of Ref. 5), the spin-flip Raman gain goes down as $B$ is increased (for a given $n_e$). On the other hand, the free-carrier absorption at the SFR scattered frequency computed from Eq. (12) goes up very rapidly as $B$ is increased, as seen in Fig. 10 for $n_e = 1.3 \times 10^{16}$ cm$^{-3}$ and $\mu = 2.4 \times 10^5$ cm$^2$/V sec. We have assumed here that $\vec{q}_s \perp \vec{B}$ and $\vec{E}_s \perp \vec{B}$, where $\vec{E}_s$ is the electric field polarization of the SFR scattered light. This assumes that the pump radiation is polarized parallel to $\vec{B}$ which is the experimental situation in most of the experiments reported here. Additional loss due to the free-carrier absorption of the pump radiation should also be considered. For a pump polarization $\vec{E}_0 \perp \vec{B}$, the $\sigma$ dependence on $B$ is stronger[5] and the Raman gain is expected to go down much faster than that for $\vec{E}_0 \| \vec{B}$ (above). The free-carrier absorption of SFR scattered light with $\vec{E}_s \| \vec{B}$ has a somewhat slower dependence[18] on $B$ than that shown in Fig. 10, but the pump radiation

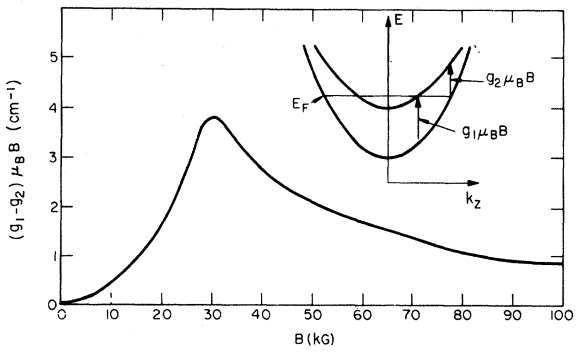


FIG. 9. Calculated nonparabolicity linewidth as a function of magnetic field for spontaneous spin-flip Raman scattering in $n_e \approx 1.3 \times 10^{16}$ cm$^{-3}$ InSb sample at $T = 0$, neglecting narrowing due to the density of states (see text).

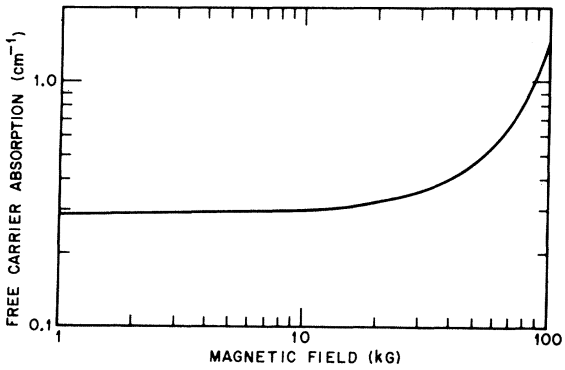


FIG. 10. Variation of free-carrier absorption in $n$-InSb as a function of magnetic field at the wavelength of SFR scattering (pump at 10.6 $\mu$) for $n$-InSb with $n_e \approx 1.3 \times 10^{16}$ cm$^{-3}$ and $\mu \approx 2.4 \times 10^5$ cm$^2$/V sec.

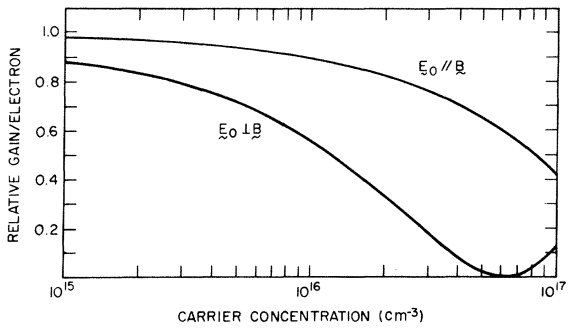


FIG. 11. Calculated relative Raman gain as a function of carrier concentration at the magnetic field required to reach the quantum limit, for $n$-InSb and for (a) $\vec{E}_0 \perp \vec{B}$ and (b) $\vec{E}_0 \parallel \vec{B}$.

now has a significantly higher free-carrier loss. Thus, qualitatively the high-field limit for the SFR laser is set jointly by decreasing $\sigma$, and increasing free-carrier absorption at the pump frequency and the SFR scattered frequency as $B$ is increased. It can also be seen, from the above discussion, that $\vec{E}_0 \parallel \vec{B}$ is a more desirable geometry compared to $\vec{E}_0 \perp \vec{B}$ geometry in spite of the higher free-carrier absorption at $\omega_s$ for $\vec{E}_0 \parallel \vec{B}$. Preliminary experiments substantiate both the above conclusions, and details will be published in the near future.

Now let us turn to the SFR power output and threshold dependence on the electron concentration. At the low $n_e$ limit, we can essentially neglect the free-carrier absorption since $B_{\min}$ is also small (see above), and thus the Raman gain has to overcome just the constant reflection losses of the Raman cavity. The $S/l\, d\Omega$ is maximum (equal to $\sigma n_e$) when we are in the quantum limit. Thus, as $n_e$ is lowered (always staying in the quantum limit) the Raman gain goes down almost linearly with $n_e$, and at some value of $n_e$, the Raman gain will not be sufficient to overcome the reflection losses. This determines the lower limit on $n_e$ for obtaining stimulated SFR scattering. This may imply that for obtaining maximum power output in the spin-flip Raman laser emission we should go to very high carrier concentrations. However, this requires high magnetic fields for reaching the quantum limit, and consequently the maximum $S/l\, d\Omega$ does not increase linearly with $n_e$ because of the $B$ dependence[5] of $\sigma$. Thus the Raman gain does not go up linearly as the carrier concentration is increased. The calculated gain [using Eq. (10)] for $\vec{E}_0 \perp \vec{B}$ and $\vec{E}_0 \parallel \vec{B}$ is shown on Fig. 11 as a function of $n_e$ choosing the magnetic field required to reach the quantum limit shown on Fig. 12. In addition, the free-carrier absorption increases with $n_e$ and $1/\tau$ and with increasing magnetic field as discussed in Eq. (12). In general, the electron collision time $\tau$ becomes shorter as $n_e$ is increased. Thus, Eq. (12) shows that the free-carrier absorption, at the magnetic field required to reach quantum limit, increases faster than linearly with $n_e$. The $n_e$ dependence of the free-carrier absorption calculated from Eq. (12) at the SFR frequency and at the magnetic field to reach quantum limit is shown on Fig. 13. Here we have used the best available mobility[27] InSb sample for each $n_e$. Hence, the slower than linear dependence of Raman gain on $n_e$, and the faster than linear dependence of total Raman cavity losses on $n_e$ (including free-carrier absorption) indicate that the optimum carrier concentration for the spin-flip Raman laser would lie at some intermediate value. Experimen-

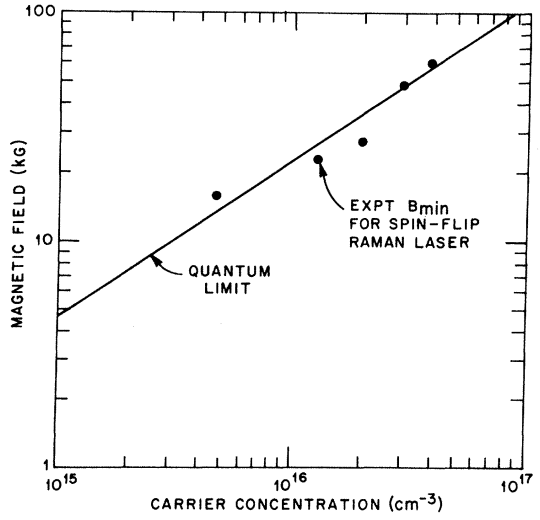


FIG. 12. The lowest magnetic field for obtaining stimulated spin-flip Raman scattering as a function of carrier concentration in InSb ($T \approx 20$ °K, $\vec{q}_e \perp \vec{B}$ noncollinear). The solid line shows theoretically calculated magnetic field necessary to reach the quantum limit.

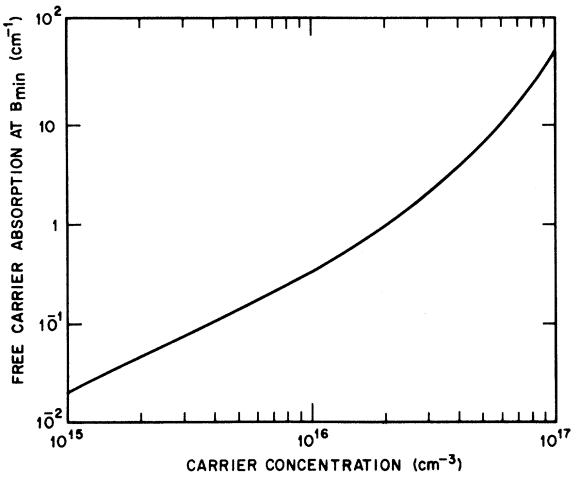


FIG. 13. Free-carrier absorption in $n$-InSb as a function of carrier concentration at the SFR scattering wavelength and at magnetic field required to reach the quantum limit (see text).

tal results show the optimum to occur at $n_e \approx 1.3\times 10^{16}$ cm$^{-3}$.

Figure 12 shows a comparison between the calculations and experiments for the lowest field at which the spin-flip Raman laser oscillation is obtained. The solid line shows the magnetic field required to reach quantum limit as a function of carrier concentration. This is the line which shows the magnetic field at which the spin-down sublevel of $l=0$ Landau level just emerges from the Fermi sea, making all the electrons available for SFR scattering. The slope is slightly larger than the expected $\frac{2}{3}$ because of the dependence of the effective mass of the electrons on the conduction band energy. The solid points show the experimentally observed $B_{min}$ (see Fig. 7) at which stimulated SFR scattering is observed. The experimental geometry is shown in in Fig. 2(a). There were no coatings on the sample. The maximum 10.6-$\mu$ pump power in the sample was ~1.5 kW. We see that there is an acceptable agreement between the lowest magnetic field at which stimulated SFR emission is observed and the magnetic field required for reaching the quantum limit. The $1.1\times 10^{15}$ cm$^{-3}$ InSb sample did not show SRS in agreement with our earlier assertion that a minimum $n_e$ is needed to exceed the cavity reflection losses. At the high concentration end, the $6\times 10^{16}$ cm$^{-3}$ InSb sample failed to show stimulated emission and is discussed below.

Figure 14 shows a plot of Raman cavity losses computed for the geometry shown in Fig. 2(a) as a function of $n_e$. (The sample dimension $l_c$ is constant in all of our samples and is $l_c = 2$ mm.) In computing this curve we have used the free-carrier absorption at the quantum limit shown in Fig. 12. The loss includes 1 Np of reflection losses which are independent of $n_e$. The calculated Raman gain (for maximum input power) is also shown on the same figure. The only adjustable parameter is the intensity in Eq. (10). This was chosen to meet the requirement that $1.1\times 10^{15}$-cm$^{-3}$ sample did not show SRS but the $4.7\times 10^{15}$-cm$^{-3}$ sample showed strong SFR laser emission. The vertical distance between the calculated gain and loss line, then, represents how far above threshold (or below) a given carrier concentration sample will be for obtaining stimulated SFR scattering in InSb at the maximum pump power $P_{in}$(max), i.e., the vertical distance between the gain and the loss curve gives theoretical values of $P_{in}(\text{max})/P_{in}(\text{threshold})$ for each concentration. We see that there are definite limits on the $n_e$ between which the stimulated SFR scattering can be obtained in agreement with the qualitative discussion earlier. On Fig. 14 we also show the experimental points for $P_{in}(\text{max})/P_{in}(\text{threshold})$ for the different carrier concentration samples. There is a qualitative agreement between theory and experiment in the low carrier concentration range but near the high concentration range, the

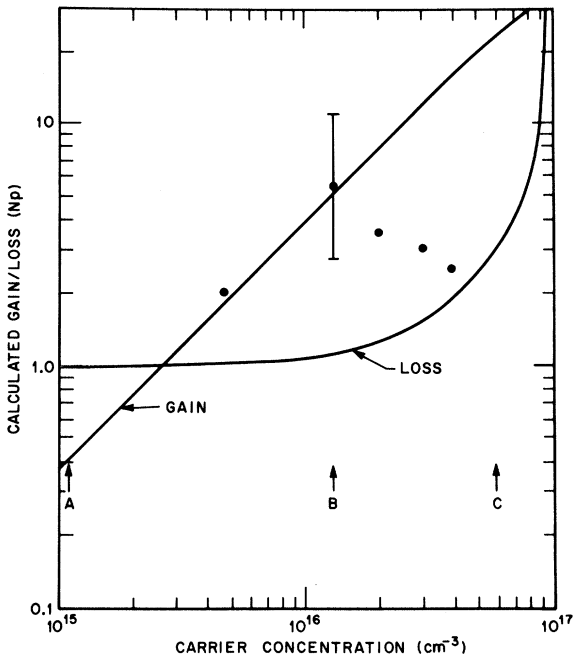


FIG. 14. Computed Raman cavity loss and spin-flip Raman gain as a function of carrier concentration in InSb. Arrows A, B, and C indicate the following: A, InSb sample which did not show stimulated spin-flip Raman scattering at the low concentration end; B, InSb sample showing the highest spin-flip Raman laser output; C, InSb sample towards the high concentration end which failed to show stimulated emission. Experimental points show $P_{in}$ (max)/$P_{in}$ (threshold) (see text).

agreement is rather poor. In particular, with the knowledge that the $4.7\times10^{15}$ cm$^{-3}$ InSb shows stimulated SFR scattering, the $6\times10^{16}$ cm$^{-3}$ InSb should also have shown SRS. Experimentally, we found otherwise. Extrapolating from the *experimental* points of $P_{in}(\max)/P_{in}(\text{threshold})$, however, we can see that the absence of stimulated SFR scattering in the $6\times10^{16}$ cm$^{-3}$ sample is not unreasonable. In addition, the theoretical curves on Fig. 14 predict the optimum concentration for stimulated SFR scattering to be $\sim4\times10^{16}$ cm$^{-3}$ in disagreement with experimental optimum concentration of $\sim1.3\times10^{16}$ cm$^{-3}$. It is possible to improve the agreement between the experiment and the theory by postulating that at threshold, the SFR laser prefers to oscillate in a totally internally reflecting bouncing-ball mode[20] which will have reflection losses less than 0.1 Np in contrast to the present 1 Np reflection loss postulated for the normal reflection Raman cavity. This possibility is under investigation and results will be published elsewhere.

## VII. APPLICATIONS OF SFR LASER

We have seen above that the spin-flip Raman laser in InSb has extremely narrow linewidth of $\leq 0.03$ cm$^{-1}$ and the linearity and resettability of fine tuning exceeds $1:3\times10^4$. The over-all tunability is from $\sim10.9$ to 13.0 $\mu$ when pumped at 10.6 $\mu$. In a sense, the SFR laser is an ideal source of tunable monochromatic coherent radiation. Together with its high peak and average power, the SFR laser should be eminently suitable for a number of practical applications such as high-resolution infrared spectroscopy, local oscillator in communication systems and radar, in systems for detection of atmospheric pollution (since some of the pollutants have IR absorption bands in the 10.9–13.0 $\mu$ range), etc.

Of all the above exciting applications, in this section we describe an attempt to evaluate the usefulness of the SFR laser as a source of monochromatic radiation in high-resolution infrared spectroscopy. We have measured the absorption of $NH_3$ in 800–900 cm$^{-1}$ range[28] using the SFR laser as the source. Figure 15 shows an outline of the experimental setup used. The SFR laser employed an $n_e\approx1.3\times10^{16}$ cm$^{-3}$ InSb sample. The rest of the setup is self-explanatory. The output gave the $NH_3$ absorption vs magnetic field which is converted to frequency using the tunability curve in Fig. 5. Figures 16 and 17 show portions of the absorption spectra of $NH_3$ (ammonia pressure $\sim$ 10–20 Torr and absorption length $\approx$ 15 cm) as a function of frequency in the

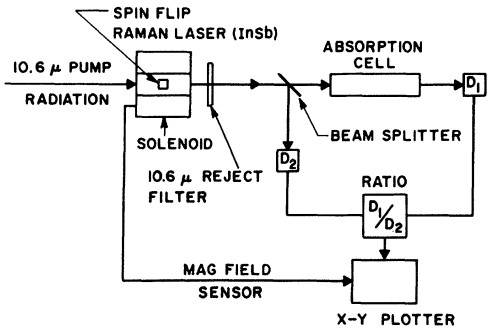


FIG. 15. Experimental setup for using the tunable spin-flip Raman laser as an infrared spectrometer source.

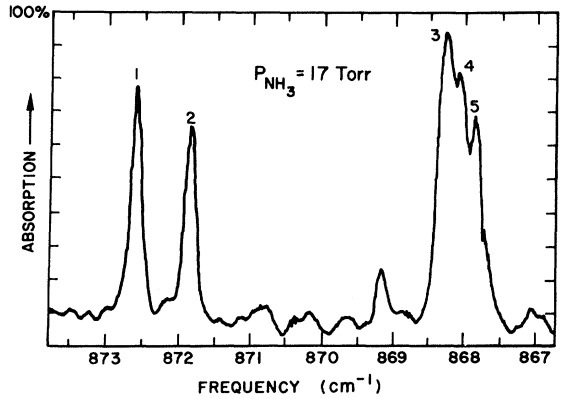


FIG. 16. Absorption spectrum of $NH_3$ at a pressure of 17 Torr taken with the spin-flip laser spectrometer shown in Fig. 14. Identifications of the transitions are as follows: transition one, $aP(3, 1)$, $sP(4, 3)$; two, $aP(3, 2)$; three, $sP(5, 0)$, $sP(5, 1)$; four, $sP(5, 2)$, $sP(5, 3)$; five, $sP(5, 4)$ (see Ref. 29).

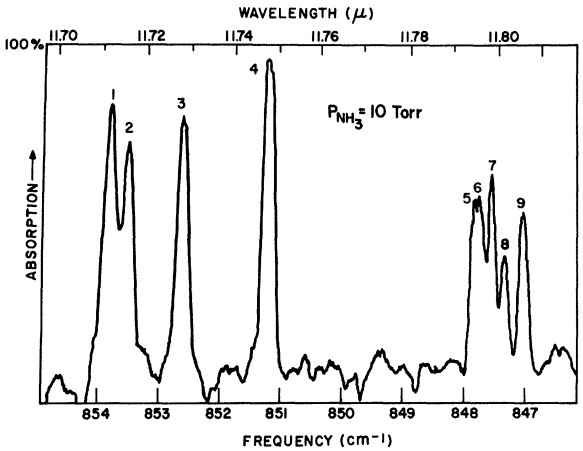


FIG. 17. Absorption spectrum of $NH_3$ at a pressure of 10 Torr taken with the spin-flip Raman laser spectrometer shown in Fig. 14. The identification of the transitions is as follows: transition one, $aP(4, 0)$; two, $aP(4, 1)$; three, $aP(4, 2)$; four, $aP(4, 3)$; five, $sP(6, 1)$; six, $sP(6, 2)$; seven, $sP(6, 3)$; eight, $sP(6, 4)$; nine, $sP(6, 5)$ (for identification, see Ref. 29).

range of 840–875 $cm^{-1}$. It should be pointed out that absolute calibration of frequency from the magnetic field is limited to ~0.1 $cm^{-1}$, but the relative calibration is better than 0.03 $cm^{-1}$. The numbers on the peaks identify[29] the transitions. The interesting point is that on Fig. 17 the $sP$ (6, 1) and $sP$ (6, 2) are resolved. The spacing is seen to be ~0.05 $cm^{-1}$. This confirms our earlier estimate of spin-flip Raman laser linewidth of $\leq$ 0.03 $cm^{-1}$. A comparison between the performance of the spin-flip laser spectrometer with that of a 15-cm conventional grating spectrometer can be obtained by studying the Figure 18 where we compare the spectrum of Fig. 17 taken by the two different techniques. The "conventional grating spectrum" is reproduced from Fig. 1(a) of Ref. 30 where the claimed resolution is ~0.1–0.2 $cm^{-1}$, and appears to be nearly the best that has been done heretofore using a conventional spectrometer. The comparison between Figs. 18(a) and 18(b) leaves no doubt about the superior resolution of the spin-flip Raman laser spectrometer.

Absorption by narrow molecular lines can be used to check the frequency stability of the SFR laser output. This was done by adjusting the magnetic field so that we were at the peak of an absorption line such as $aP$ (4, 3) and monitoring the absorption at a low $NH_3$ pressure of $\lesssim$ 1 Torr for a period of 30 min. There was no measurable change in the absorption indicating that the frequency stability of the spin-flip Raman laser is at least as good as the estimated linewidth of Raman laser emission, i.e., 0.03 $cm^{-1}$ or ~$1:3\times10^4$.

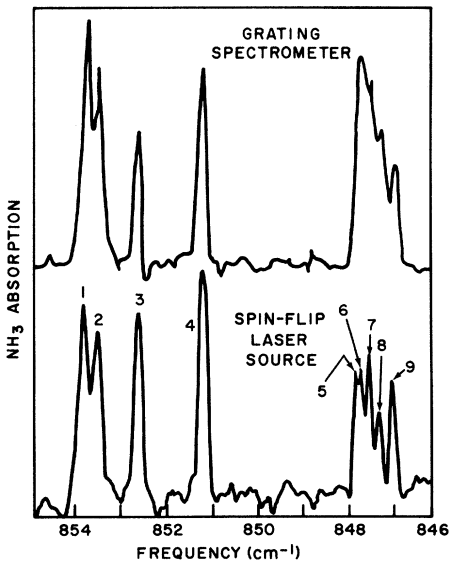


FIG. 18. Comparison of absorption spectrum in Fig. 16 taken with (a) the spin-flip laser and (b) conventional grating spectrometer reproduced from Ref. 30.

The ultimate resolution possible with the spin-flip Raman laser spectrometer is expected to be much better than what we have shown so far. This is so because the emission linewidth of a quantum oscillator such as the spin-flip Raman laser is expected to be significantly narrower[21] than the present upper limit of 0.03 $cm^{-1}$ reported here. For further details of spectroscopy using a spin-flip Raman laser, Ref. 31 should be consulted.

An additional advantage of the spin-flip Raman laser spectrometer lies in the fact that the output occurs in form of ~30 nsec wide pulses in normal operation (or ~3 nsec wide pulses in mode-locked operation) as seen in Fig. 6. This should allow time resolved spectroscopy in the 10-14 $\mu$ range which heretofore has not been possilbe with high resolution. The drawback of a limited tuning range of spin-flip Raman laser could be overcome by using different pump lasers, higher magnetic fields and other narrower band-gap semiconductors (in place of InSb) such as $Pb_{1-x}Sn_xTe$ or $Hg_{1-x}Cd_xTe$ where the $g$ value of the conduction electrons is larger than that in InSb.

## VIII. CONCLUSION

The recent success of obtaining stimulated Raman scattering from spin-flip of conduction electrons in InSb indicates the importance of Raman scattering processes from mobile carriers in semiconductors for obtaining tunable coherent radiation in the infrared. We have described some of the physics underlying the InSb spin-flip Raman laser in detail and touched upon possible applications of such a tunable source. The other tunable source in this range of wavelength is the $Pb_{1-x}Sn_xTe$ diode laser[24] which can be gross tuned by changing the composition and fine tuned by changing the current. However, the fine tuning of the $Pb_{1-x}Sn_xTe$ diode laser is far from ideal. Unlike the extremely linear and continuous tuning of the SFR laser described here, the $Pb_{1-x}Sn_xTe$ diode laser tuning occurs in jumps from one cavity mode to the next (with a small amount of fine tuning about each cavity mode). Thus, the SFR laser has some merit over the diode lasers. With the operation of the spin-flip Raman laser, we have just barely scratched the surface of the field of stimulated Raman scattering from free carriers in semiconductors. The field is wide open and in what follows we make a few suggestions for promising future research:

(a) Sparked by the success of stimulated Raman scattering from spin-flip of electrons in InSb, the next fruitful direction is to look for SRS arising from some of the other electron processes discussed earlier in the paper. Of these Raman processes, at least some can be made to go stimulated using currently available pump lasers. In particular, the plasmon Raman scattering in InAs and InSb

as well as the spin-flip Raman scattering in PbTe appear to be very exciting.

(b) The SRS from mobile carriers in semiconductors is a technique for creating a large perturbation of the electron gas. Such large perturbations may be helpful in studying nonlinear plasma effects in solids. For example, we are saturating the spin system during SRS from spin-flip of electrons in InSb. Another example is possible SRS from spin flip of electrons in a multivalley semiconductor such as PbTe. Here, by proper choice of the crystal orientation, it might be possible to set up an instability involving intervalley electron transfer during SRS from the spin-flip process. This "sloshing" type of instability may be detectable.

(c) Improving the characteristics of the SFR laser appears to be a promising direction. The cw operation of the SFR laser should be possible with properly coated InSb samples. The cw operation will significantly improve the linewidth of the output and increase the applications of the spin-flip Raman laser. Efforts should also be made to increase the output power from the SFR laser by changing the spin-relaxation time and/or by drifting the carriers. Heterodyne spectroscopy to measure the exact width of the SFR laser output will also be useful.

(d) It should be possible to increase the tuning range of the SFR laser by (i) using materials with larger $g$ values, e.g., $Pb_{1-x}Sn_xTe$ or $Hg_{1-x}Cd_xTe$; (ii) using higher magnetic fields; and (iii) using different pump laser frequencies, e.g., pumping at 9.6 $\mu$ using the $CO_2$ laser $00^01 - 02^00$ transitions[22] should allow tuning down to 9.8 $\mu$; pumping at 11.00 $\mu$ using an $N_2O$ laser[22] should allow us to go to ~13.6 $\mu$; pumping at 5.5 $\mu$ using a CO laser[22] should allow us to tune from 5.8 to 6.6 $\mu$; pumping at 23 $\mu$ using a $H_2O$ laser should allow us to go in the 30–40 $\mu$ range, etc.

(e) There are several unanswered questions about the spin-flip Raman laser in InSb. For example, the fine-tuning characteristics of the SFR laser which are very desirable are not well understood, nor is the understanding of the carrier concentration dependence of the SFR laser output quantitative. These problems need future attention.

(f) Finally, there is a class of tunable Raman scattering processes which do not depend upon the magnetoplasma for scattering strength but derive their tunability from the magnetoplasma. One such process is the polariton scattering in the presence of a magnetoplasma[32] in GaAs. This process appears promising for obtaining tunable SRS in the near infrared.

(g) Nonlinear optical effects with the tunable SFR laser appear possible because of its relatively high tunable power output. For example, second harmonic generation from SFR laser frequency will yield a new tunable source of monochromatic radiation in the 5.4–6.5 $\mu$ range. As another example, difference frequency mixing between a 10.6 $\mu$ laser and the tunable SFR laser will lead to tunable coherent monochromatic power output in the far infrared in the 30–170 $cm^{-1}$ range and will be of considerable importance in the far-infrared spectroscopy, because the difference frequency output will retain all the characteristics of the monochromaticity and the linearity of tuning of the SFR laser.

## ACKNOWLEDGMENTS

We would like to thank Dr. P. A. Wolff and Dr. Y. Yafet for their critical comments on the manuscript, R. J. Kerl for technical assistance, and A. Albert for polishing the crystals.

[1]C. K. N. Patel and E. D. Shaw, Phys. Rev. Letters 24, 451 (1970).

[2]P. M. Platzman, Phys. Rev. 139, A379 (1965).

[3]A. L. McWhorter, in *Physics of Quantum Electronics*, edited by P. L. Kelley, B. Lax, and P. E. Tannenwald (McGraw-Hill New York, 1966), p. 111.

[4]P. A. Wolff, Phys. Rev. Letters 16, 225 (1966).

[5]Y. Yafet, Phys. Rev. 152, 858 (1966).

[6]A. Mooradian and G. B. Wright, Phys. Rev. Letters 16, 999 (1966); A. Mooradian and A. L. McWhorter, *ibid.* 19, 849 (1967); B. Tell and R. J. Martin, Phys. Rev. 167, 381 (1968).

[7]C. K. N. Patel and R. E. Slusher, Phys. Rev. 167, 413 (1968).

[8]C. K. N. Patel and R. E. Slusher, Phys. Rev. Letters 21, 1563 (1968).

[9]R. E. Slusher, C. K. N. Patel, and P. A. Fleury, Phys. Rev. Letters 18, 77 (1967).

[10]C. K. N. Patel, in *Modern Optics* (Polytechnic Press, Brooklyn, N. Y., 1967), Vol. XVII, pp. 19–51.

[11]G. B. Wright, P. L. Kelley, and S. H. Groves, in *Light Scattering Spectra of Solids*, edited G. B. Wright (Springer-Verlag, New York, 1969), pp. 335–343.

[12]W. D. Johnston, Jr. and I. P. Kaminow, Phys. Rev. 168, 1045 (1968); 178, 1528 (E) (1969), and references cited herein; W. D. Johnston, Jr., I. P. Kaminow, and J. G. Bergman, Jr., Appl. Phys. Letters 13, 190 (1968).

[13]C. K. N. Patel and R. E. Slusher, Phys. Rev. 177, 1200 (1969).

[14]A. J. Beaulieu, Appl. Phys. Letters 16, 504 (1970).

[15]A. E. Hill, Appl. Phys. Letters 12, 324 (1968).

[16]J. G. Skinner and W. G. Nilsen, J. Opt. Soc. Am. 58, 113 (1968); E. P. Ippen, Appl. Phys. Letters 16, 303 (1970).

[17]C. K. N. Patel, Appl. Phys. Letters 7, 246 (1965); R. M. Osgood, Jr. and W. C. Eppers, Jr., *ibid.* 13, 409 (1968); R. M. Osgood, Jr., E. R. Nichols, W. C. Eppers, Jr., and R. D. Petty, *ibid.* 15, 69 (1969).

[18]E. D. Palik and G. B. Wright, in *Optical Properties of III-V Compounds*, edited by R. K. Willardson and A. C. Beer (Academic, New York, 1966), Vol. III, pp.

159–202.

[19]C. K. N. Patel and E. D. Shaw (unpublished).

[20]R. J. Collins and J. A. Giordmaine, in *Quantum Electronics*, edited by P. Grivet and N. Bloembergen (Columbia U. P., New York, 1964), Vol. III, pp. 1239–1246.

[21]C. H. Townes, in *Advances in Quantum Electronics*, edited by J. R. Singer (Columbia U. P., New York, 1961), p. 3; see also, W. R. Bennett, Jr., Appl. Opt. Suppl. 1, 24 (1962).

[22]For a review of $CO_2$ lasers and the transitions seen in laser oscillation see C. K. N. Patel, J. Chim. Phys. 64, 87 (1967). See also, C. K. N. Patel, in *Advances in Lasers*, edited by A. K. Levine (M. Dekker, New York, 1968), Vol. II, p. 1.

[23]M. Born and E. Wolf, *Principles of Optics*, 2nd ed. (Pergamon, New York, 1959).

[24]E. D. Hinkley and T. C. Harman, Appl. Phys. Letters 13, 49 (1968); see also E. D. Hinkley, *ibid.* 16, 351 (1970).

[25]L. M. Roth and P. N. Argyres, in *Physics of III-V Compounds*, edited by R. K. Willardson and A. C. Beer (Academic, New York, 1966), Vol. I, pp. 159–202.

[26]V. P. Makarov, Zh. Eksperim. i Teor. Fiz. Pis'ma v Redaktsiyu 55, 704 (1968) [Soviet Phys. JETP Letters 28, 366 (1969)]; B. S. Wherrett and P. G. Harper, Phys. Rev. 183, 692 (1969).

[27]The InSb samples had the following characteristics (77 °K): (a) $n_e = 1.1\times10^{15}$ cm$^{-3}$, $\mu = 3\times10^5$ cm$^2$/V sec; (b) $n_e = 4.7\times10^5$ cm$^{-3}$, $\mu = 2\times10^5$ cm$^2$/V sec; (c) $n_e = 1.3\times10^{16}$ cm$^{-3}$, $\mu = 2.4\times10^5$ cm$^2$/V sec; (d) $n_e = 2\times10^{16}$ cm$^{-3}$, $\mu = 1\times10^5$ cm$^2$/V sec; (e) $n_e = 3\times10^{16}$ cm$^{-3}$, $\mu = 1\times10^5$ cm$^2$/V sec; (f) $n_e = 4\times10^{16}$ cm$^{-3}$, $\mu = 1\times10^5$ cm$^2$/V sec; and (g) $n_e = 6\times10^{16}$ cm$^{-3}$, $\mu = 7\times10^4$ cm$^2$/V sec.

[28]*Tables of Wave Numbers for the Calibration of Infrared Spectrometers* (Butterworths, London, 1961), p. 671.

[29]J. S. Garing, H. H. Nielsen, and K. N. Rao, J. Mol. Spectry. 3, 496 (1959).

[30]H. M. Mould, W. C. Price, and G. R. Wilkinson, Spectrochim. Acta 13, 313 (1959).

[31]C. K. N. Patel, E. D. Shaw, and R. J. Kerl, Phys. Rev. Letters, 25, 8 (1970).

[32]C. K. N. Patel and R. E. Slusher, Phys. Rev. Letters 22, 282 (1969).

PHYSICAL REVIEW B VOLUME 3, NUMBER 4 15 FEBRUARY 1971

# Plasmon-Phonon Interference in CdS†

J. F. Scott* and T. C. Damen

*Bell Telephone Laboratories, Holmdel, New Jersey* 07733

and

J. Ruvalds and A. Zawadowski‡

*Department of Physics, University of Virginia, Charlottesville, Virginia* 22901

(Received 18 September 1970)

The Raman spectra of plasmons in In- and Ga-doped cadmium sulfide are shown to consist of very asymmetric peaks. A prominent interference shape is exhibited which is very similar to that manifested by anharmonic phonon interactions between two optical phonons, as in $AlPO_4$ and $BaTiO_3$. In the present case, the interaction between the heavily damped plasmon mode and one longitudinal optical phonon is due to the Coulomb interaction. The interference features of the Raman spectrum are related to the electronic (plasmon) and ionic (phonon) charge-density correlation functions, where the ionic charge is multiplied by a factor to include the nonionic (electronic) part of the light-phonon scattering amplitude. In other words, we treat the spectrum as due to interfering amplitudes for scattering into the plasmon state $\langle \mathrm{PL}|$ via two channels: one direct, $\langle \mathrm{PL}|\alpha|0\rangle$; and one via an intermediate LO-phonon state coupled by the Coulomb interaction, $\langle \mathrm{PL}|\,\mathrm{Coul.}\,|\mathrm{LO}\rangle \times \langle \mathrm{LO}|\alpha|0\rangle$. This calculation gives very good agreement with the observed line shape, and demonstrates the inadequacy of treating the spectrum in terms of the usual dielectric function. In the special case when the light-phonon scattering is purely ionic, however, our Green's-function calculation is shown to be equivalent to the dielectric-function formulation which includes both the plasmon and phonon contributions. A detailed comparison of our theory with the experimental spectrum yields an estimate of the relative contributions to the light-phonon scattering amplitude from electronic and ionic charges. For CdS, these contributions are found to be of the same order of magnitude, but opposite in sign.

## I. INTRODUCTION AND EXPERIMENTAL

Very recent experiments[1] on inelastic light scattering from plasmons in CdS revealed several anomalies: First, the plasmon line shape was somewhat asymmetric; second, the plasmon linewidth was 25% narrower than calculated from measured Hall mobilities; third, relatively featureless scattering in the 0–200-cm$^{-1}$ region assigned as noncollective electron transitions[2] ("single-particle scattering") occurred for both trace and off-diagonal polarizabilities, whereas the trace scattering is ex-

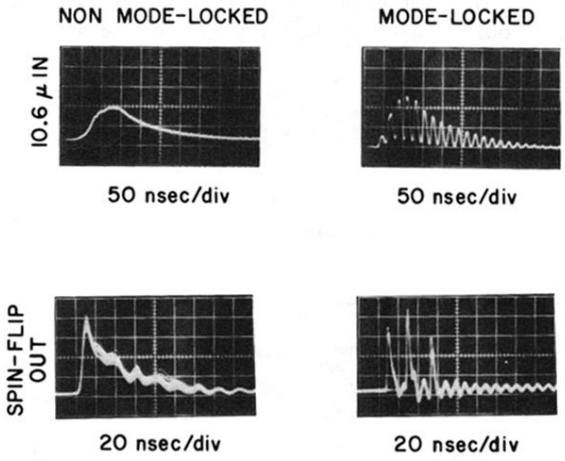


FIG. 6. Input $CO_2$ laser pulses and output spin-flip Raman laser pulses for normal operation and for mode-locked operation of the $CO_2$ laser ($n$-InSb, $n_e \approx 1.3\times10^{16}$ cm$^{-3}$, $T \approx 18$ °K, $B \approx 40$ kG).